measured by time-resolved terahertz spectroscopy. *Phys. Rev. B* **62,** 15764–15777 (2000).
13. Lövenich, R., Lai, C. W., Hägele, D., Chemla, D. S. & Schäfer, W. Semiconductor polarization dynamics from the coherent to the incoherent regime: Theory and experiment. *Phys. Rev. B* **66,** 045306 (2002).
14. Nuss, M. C. & Orenstein, J. in *Millimeter and Submillimeter Wave Spectroscopy of Solids* (ed. Grüner, G.) 7–50 (Springer, Berlin, 1998).
15. Dressel, M. & Grüner, G. *Electrodynamics in Solids* 61–62 (Cambridge Univ. Press, Cambridge, 2002).
16. Haug, H. & Koch, S. W. *Quantum Theory of the Optical and Electronic Properties of Semiconductors* (World Scientific, Singapore, 1994).
17. Gerlach, B., Wüsthoff, J., Dzero, M. O. & Smondyrev, M. A. Exciton binding energy in a quantum well. *Phys. Rev. B* **58,** 10568–10577 (1998).
18. Tzoar, N. & Platzman, P. M. High-frequency conductivity of a two-dimensional, two-component electron gas. *Phys. Rev. B* **20,** 4189–4193 (1979).
19. Wegener, M. *et al.* Femtosecond dynamics of excitonic absorption in the infrared $In_xGa_{1-x}As$ quantum wells. *Phys. Rev. B* **39,** 12794–12801 (1989).
20. Selbmann, P. E., Gulia, M., Rossi, F., Molinari, E. & Lugli, P. Coupled free-carrier and exciton relaxation in optically excited semiconductors. *Phys. Rev. B* **54,** 4660–4673 (1996).
21. Siantidis, K., Axt, V. M. & Kuhn, T. Dynamics of exciton formation for near band-gap excitations. *Phys. Rev. B* **65,** 035303 (2002).
22. Oh, I. K. Exciton formation assisted by LO phonons in quantum wells. *Phys. Rev. B* **62,** 2045–2050 (2000).
23. Betz, M. *et al.* Nonlinear optical response of highly energetic excitons in GaAs: Microscopic electrodynamics at semiconductor interfaces. *Phys. Rev. B* **65,** 085314 (2002).
24. Siarkos, A., Runge, E. & Zimmermann, R. Center of mass properties of the exciton in quantum wells. *Phys. Rev. B* **61,** 10854–10867 (2000).
25. Damen, T. C. *et al.* Dynamics of exciton formation and relaxation in GaAs quantum wells. *Phys. Rev. B* **42,** 7434–7438 (1990).
26. Blom, P. W. M., van Hall, P. J., Smit, C., Cuypers, J. P. & Wolter, J. H. Selective exciton formation in thin $GaAs/Al_xGa_{1-x}As$ quantum wells. *Phys. Rev. Lett.* **71,** 3878–3881 (1993).
27. Deveaud, B., Sermage, B. & Katzer, D. S. Free exciton versus free carrier luminescence in a quantum well. *J. Phys. Colloq. C* **5,** 11–14 (1993).
28. Kumar, R., Vengurlekar, A. S., Prabhu, S. S., Shah, J. & Pfeiffer, L. N. Picosecond time evolution of free electron-hole pairs into excitons in GaAs quantum wells. *Phys. Rev. B* **54,** 4891–4897 (1996).
29. Landau, L. & Zeldovich, J. On the relation between the liquid and gaseous states of metals. *Acta Physicochim. USSR* **XVIII** 2–3, 194–196 (1943).
30. Mott, N. F. *Metal Insulator Transitions* (Taylor and Francis, London, 1990).

Acknowledgements We thank J. Reno for growth of the quantum well samples, and S. L. Chuang for band-structure calculations. We also thank M. Kira, S. W. Koch, M. Woerner, T. Timusk and J. Orenstein for discussions. This work was supported by the Office of Basic Energy Sciences of the US Department of Energy, the Deutsche Forschungsgemeinschaft and the Alexander von Humboldt Foundation.

Competing interests statement The authors declare that they have no competing financial interests.

Correspondence and requests for materials should be addressed to R.A.K. (RAKaindl@lbl.gov).

The 'zero charge' partitioning behaviour of noble gases during mantle melting

R. A. Brooker*, Z. Du*†, J. D. Blundy*, S. P. Kelley‡, N. L. Allan†, B. J. Wood*, E. M. Chamorro*§, J.-A. Wartho‡§ & J. A. Purton‖

* *CETSEI, Department of Earth Sciences, University of Bristol, Wills Memorial Building, Bristol BS8 1RJ, UK*
† *School of Chemistry, University of Bristol, Cantock's Close, Bristol BS8 1TS, UK*
‡ *Department of Earth Sciences, Open University, Walton Hall, Milton Keynes MK7 6AA, UK*
‖ *CLRC, Daresbury Laboratory, Warrington, Cheshire WA4 4AD, UK*

Noble-gas geochemistry is an important tool for understanding planetary processes from accretion to mantle dynamics and atmospheric formation[1–4]. Central to much of the modelling of such processes is the crystal–melt partitioning of noble gases during mantle melting, magma ascent and near-surface degassing[5]. Geochemists have traditionally considered the 'inert' noble gases to be extremely incompatible elements, with almost 100 per cent extraction efficiency from the solid phase during melting processes. Previously published experimental data on partitioning between crystalline silicates and melts has, however, suggested that noble gases approach compatible behaviour, and a significant proportion should therefore remain in the mantle during melt extraction[5–8]. Here we present experimental data to show that noble gases are more incompatible than previously demonstrated, but not necessarily to the extent assumed or required by geochemical models. Independent atomistic computer simulations indicate that noble gases can be considered as species of 'zero charge' incorporated at crystal lattice sites. Together with the lattice strain model[9,10], this provides a theoretical framework with which to model noble-gas geochemistry as a function of residual mantle mineralogy.

Extreme incompatibility is a basic tenet of most geochemical models for mantle degassing, whereby primordial isotopes such as ^{3}He and ^{36}Ar are removed from the mantle and replaced by daughter products, ^{4}He and ^{40}Ar, through *in situ* radioactive decay from residual U, Th and K, which are assumed to be less incompatible. Variations in ^{3}He/^{4}He and ^{36}Ar/^{40}Ar ratios in lavas have long been used to argue for a layered mantle in which mid-ocean-ridge basalts (MORB) sample an upper, depleted and degassed layer characterized by low ^{3}He/^{4}He and ^{36}Ar/^{40}Ar ratios, while ocean island basalts (OIB) come from an isolated, undegassed lower (undepleted or 'primordial') layer with much higher ratios[1,2,4]. However, this two-layer model has become increasingly difficult to reconcile with independent evidence suggesting whole-mantle convective mixing[11] and tomographic images of subducted slabs in the lower mantle[12]. There are also concerns related to models of the Earth's radiogenic heat budget[13], the observation of higher noble-gas abundances in MORB (degassed source) than in OIB (undegassed source)[14] and the distribution of He isotopes between these two 'source reservoirs'[15]. Consequently, the behaviour of noble gases during mantle melting must be established with some certainty in order to constrain future models of mantle geodynamics.

Our ability to model noble gases during mantle melting is severely compromised by our ignorance of the mechanisms by which noble-gas atoms are incorporated into crystals. There is a widespread view that, unlike trace cations which can clearly enter

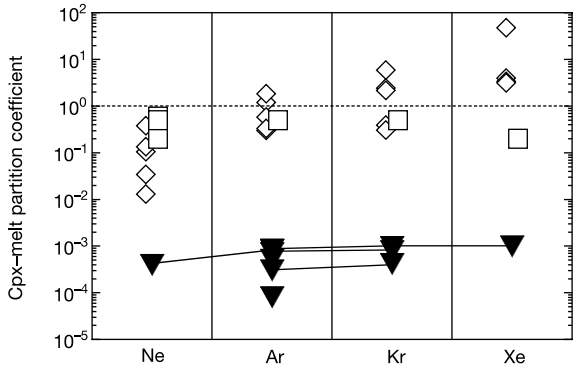

Figure 1 Experimental cpx–melt partition coefficients for noble gases. Values determined for this study using UVLAMP analysis (filled inverted triangles) have errors approximately within the symbols. Data from similar experimental conditions are joined by solid lines. These results are compared to previous experiments using bulk analytical techniques from Hiyagon and Ozima[6] (open squares) and Broadhurst *et al.*[5,7] (open diamonds). The higher, but parallel, trend observed by Hiyagon and Ozima is the expected consequence of melt contamination, as noted by those authors. Similar results were reproduced, but rejected in this study (see Methods). The systematic fractionation of light over heavy noble gases and D values >1 for the Broadhurst *et al.*[7] data appear to be an artefact of adsorbed or trapped gas in their crystals, as discussed in ref. 18.

§ Present addresses: Ecole Normale Superieure de Lyon, 46 Allée d'Italie, Lyon Cedex 7, 69364 France (E.M.C.); School of Applied Geology, Curtin University, GPO Box U1987, Perth WA 6001, Australia (J.-A.W.).

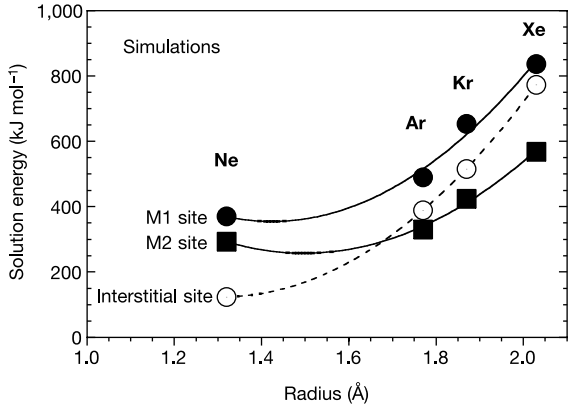

Figure 2 Calculated solution energies for noble gases in interstitial positions or lattice sites in jadeite (see Methods). Noble-gas radii in 8-fold coordination are taken from ref. 29.

lattice sites, the 'inert' noble gases reside at extended defects, intrinsic defects or grain boundaries, and are therefore not subject to the same thermodynamic controls on crystal–melt partitioning. The situation is not helped by comparison of measurements showing incompatible behaviour for natural samples[16,17], with contrasting compatible behaviour in early experiments[5–8]. The lack of any theoretical framework for noble-gas incorporation into crystals precludes a critical evaluation of these sparse and disparate crystal–melt partitioning data. In this study we present new experimental clinopyroxene–melt partitioning data for a suite of trace elements including Ne, Ar, Kr and Xe. In addition, we also perform an independent set of atomistic simulations to compare with the experimental results. The data for noble gases are then evaluated along with data for other trace cations to determine if trends observed for each isovalent series can be extrapolated to 'zero charge' for the noble gases.

In the experiments, clinopyroxene (cpx) crystals with compositions along the diopside (Di) to jadeite (Jd) solid-solution join were grown from silicate melts doped with a cocktail of trace cations at the 10–1,000 p.p.m. level. Details of experiments are given in Methods, and compositions of crystals and melts are given in Supplementary Information. The concentrations of trace cations in crystals and melt were determined by standard ion-probe techniques, while Ne, Ar, Kr and Xe were measured using an ultraviolet laser ablation microprobe (UVLAMP) technique[18,19]. Nernst partition coefficients (D), calculated as the weight concentration ratio of an element in the crystal to that in the melt, are reported in Supplementary Information.

Comparisons of our new UVLAMP results with previously published data for noble gases are shown in Fig. 1. This figure illustrates the relatively low and constant partition coefficient at $\sim 10^{-3}$–10^{-4} over a range of cpx composition, pressure (0.1–8.1 GPa) and temperature (1,200–1,665 °C). The discrepancies between the UVLAMP results and older data sets are almost certainly related to the advantages of our new micro-analytical technique in identifying and avoiding fluid or melt inclusions in the crystals, confirming reservations expressed in early studies[6,16,17,20].

Further support for our lower partition coefficients comes from atomistic computer simulations that follow the approach used in earlier studies of cation incorporation[21]. These calculations evaluate the defect energy, and thus the solution energy associated with the substitution of a noble-gas atom, either on an M1 or M2 site or at an interstitial position in cpx (see Methods).

Calculated solution energies[21] (Fig. 2) indicate that Ar, Kr and Xe substitute at the M2 site in jadeite (and diopside; not shown) rather than the M1 site. The lowest solution energies, which correspond to the highest mineral–melt D values, involve compensating defects at adjacent M1 sites (for example, Ti^{4+} for Al^{3+} in jadeite). For Ne, the simulations suggest that an interstitial position is preferred to M1 or

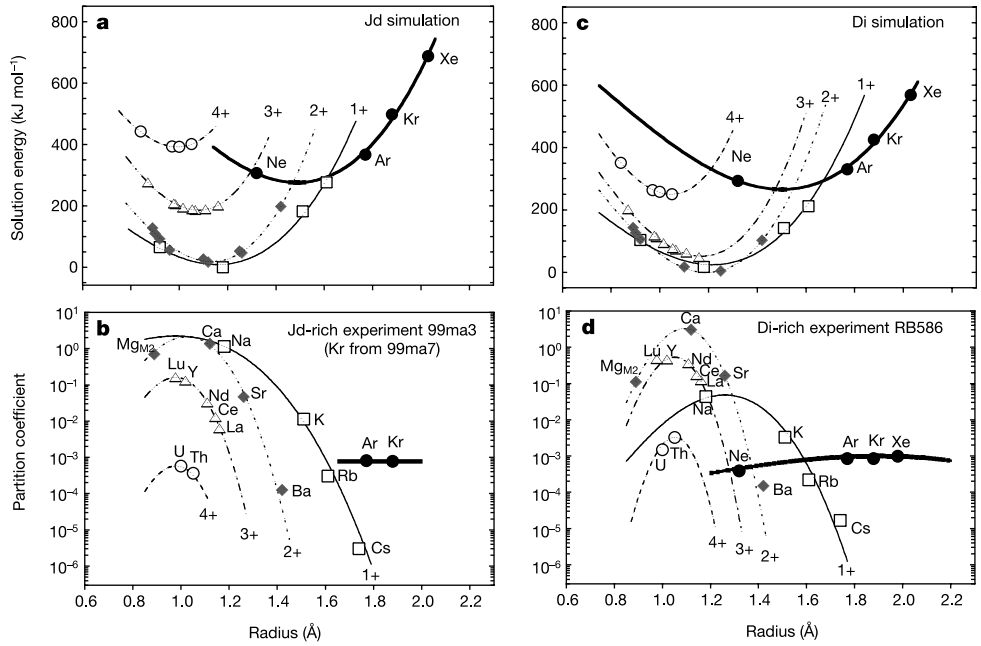

Figure 3 Computational and experimentally determined Onuma-type[30] diagrams for cpx partitioning. The experimental partition coefficients (**b**, **d**) and the calculated solution energies for substitution on the M2 site (**a**, **c**) for each isovalent series of trace elements are plotted against radius[29,31] to show the near-parabolic relationships. Simulated solution energies at M2 (in order of increasing ionic radius) are shown for the noble gases (including Ne at M2); 1 + cations Li, Na, K, Rb; 2 + cations Mg, Co, Fe, Mn, Cd, Ca, Eu, Sr, Ba; 3 + cations Sc, Lu, Yb, Ho, Gd, Eu, Nd, La; and 4 + cations Zr, Ce, U, Th. The curves through each isovalent series for the simulations and experiments have been fitted to the lattice strain equations of Brice[9,10,22] (see Methods), except for the limited experimental 4+ data where the fit has been forced through the data points using a proportionate value of E (see Fig. 4 legend). Similar trends are seen in the other experiments of this study and the derived parameters, E, r_0 and D_0, are presented in Supplementary Information. The curve through the noble gases in **d** is a fitted parabola, but the limited data in **b** are connected by a straight line. Error bars have been omitted for clarity, but are available in Supplementary Information.

M2. In Fig. 3, the partition coefficients for cations that prefer the M2 site are plotted as a function of ionic radius, and compared with those for the noble gases. Data from selected experiments are compared with simulations for pure jadeite and diopside cpx compositions. Both the experimental and simulated data show the expected approximately parabolic dependence on ionic radius for each isovalent series[9,10]. It is also clear that the curvature of the parabolae decreases with decreasing cation charge as shown previously[9]. The parabola fitted through the noble-gas data in Fig. 3d is consistent with this trend. The openness of the parabolic fit to experimental data compared to that of the simulations in Fig. 3 is most likely to be a consequence of either the difference in site stiffness due to the much lower temperatures for the calculations (in the static limit) compared with the experiments or some simplifying assumptions made for the simulated melt environment. Both experimental and simulated data suggest that the partition coefficients (or solution energies) for noble gases are approximately the same as for the 4 + cations (U and Th), as predicted in ref. 10. The various lines of agreement between simulations and experiments are remarkable, and argue strongly that lattice site energetics exercise the most important control on partitioning of all species irrespective of charge.

Finally, we consider the simulated and experimental data in terms of the Brice equation[22] and the lattice strain model[9,10]. This equation and model, taken together, predict that, at a given pressure and temperature, the primary thermodynamic controls on partitioning are the elastic and electrostatic work required at a crystal lattice site to accommodate a cation that is different in size and/or charge to the host cation normally resident at that site (see Methods). This approach involves three parameters for each set of isovalent cations entering a given lattice site[9]: r_0, the optimum radius of the site; E, the apparent or effective Young's modulus of the site, which controls its tolerance of misfit cations; and D_0, the partition coefficient for a (fictive) cation with radius r_0. These parameters can then be modelled as a function of pressure and temperature (and melt composition) as described in Methods. The charge mismatch can be thought of as the 'effective' site charge after substitution, that is, the charge difference between the substituent ion (or species) and the charge at the site in the undoped crystal.

The data in Fig. 4 show that observations made for all three parameters as a function of cation charge can be extended to zero charge for the noble gases. In Fig. 4a, E decreases linearly as the charge on the substituent decreases. In Fig. 4b, D_0 varies parabolically with charge, with a maximum value at the optimum average site charge (that is, zero effective charge), which is between 2 + and 1 + depending on the diopside:jadeite ratio. The value of D_0 for an effective charge of 2 − (that is, the noble gases) is very similar to that for 2 + (that is, U^{4+} and Th^{4+}), as predicted in ref. 10. Accurate determination of r_0 becomes very difficult as the parabolae become more open, but a general increase with decreasing charge is apparent in Fig. 4c. The behaviour of D_{Ne} in Figs 3 and 4 remains inconclusive. The data could be consistent with Ne occupying the M2 site, Ne at interstitial positions (Fig. 2) with partitioning characteristics similar to M2, or Ne may sit on both M2 and the smaller M1 site. The last two options may increase D_{Ne} and artificially decrease the fitted value of E for M2 (that is, to give a more open parabola). However, the constraints provided by the heavier noble gases would still produce the general trends observed in Fig. 4.

The consistency of these systematic trends strongly suggests that noble gases enter crystal lattices in just the same way as cations, causing lattice strains due to the mismatch of size and charge. It is this effective charge which gives the 'inert' noble gases their apparent 'crystal chemistry'. It is unlikely that our observations would be followed if noble gases did not enter lattice sites. For example, interstitial incorporation for all the noble gases would produce different trends in r_0 and E compared with values obtained by extrapolation from those for cations. Another possibility is incorporation at extended defects: this would result in a continuous

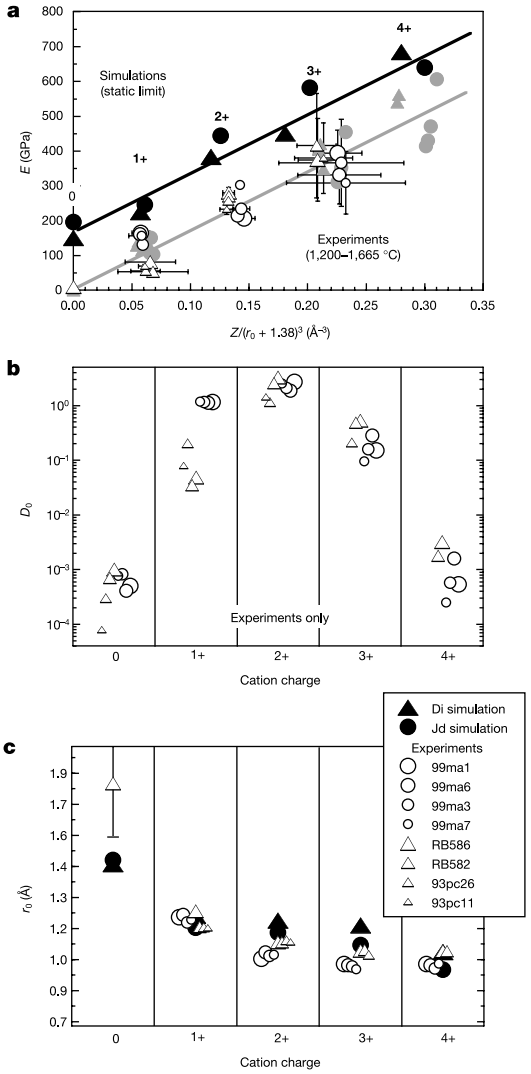

Figure 4 Comparison of lattice strain model parameters. Data derived from both simulations (filled black symbols) and experiments (open symbols) are plotted as a function of charge on the substituent species: **a**, E, the apparent site Young's modulus; **b**, D_0, the partition coefficient for a cation with ideal radius r_0; and **c**, r_0, the optimum site radius. Triangles are Di-rich samples, circles Jd-rich. In **a**, E is plotted against the ratio of charge to site volume (d^3), where $d = r_0 + 1.38$ Å (the ionic radius of O^{2-}; ref. 31). The E values for the unconstrained fitted parabola through 1 + , 2 + and 3 + cation trends and the noble gases in Fig. 3d are shown as open symbols in **a**, error bars reflecting the range of possible fits through the analytical errors on measured partition coefficients. However, it is not possible to constrain a parabola through the two experimental 4 + data points. An alternative approach is to fit the data by using the values of E for the best-defined parabola (2 +), and calculating 1/2, 3/2 or 4/2 times this value for 1 + , 3 + and 4 + , respectively[9]. These fits are shown as grey symbols in **a**, and there is good agreement between the E values derived by each method. These proportionate 4 + E values are used to fit the experimental data for 4 + cations in Fig. 3b and d, and in **b** and **c** of this figure. Differences between experimental and simulation data trends reflect the difference in temperature between the two data sets (static limit versus 1,200–1,665 °C) and the simplifying assumptions about melt environment used in the simulations. In **b**, D_0 shows an approximately parabolic dependence on charge[10]. The variation in peak position for different experiments reflects variation in optimum M2-site charge from 1 + (jadeite) to 2 + (diopside). In **c**, r_0 is seen to generally increase with decreasing charge. Parabola shape and peak positions are generally difficult to constrain, as data are biased towards the large radii limb of the parabola. This is further compounded for the noble gases by the low curvature of the parabola, and a representative large error bar has been included in **c**.

decrease in partition coefficient with increasing atomic size, as observed for noble-gas adsorption[6,18]. Incorporation at intrinsic defects is not a viable mechanism for the noble-gas concentration range in our experiments (~0.01–0.5 p.p.m.).

The ability to consider noble gases as 'zero charge' cations represents an advance in our capability to model heavy noble gas behaviour during mantle melting. Noble gases need not be viewed as 'special cases' with partitioning behaviour dominated by intractable defect-controlled or grain-boundary processes. Comprehensive modelling of noble gases during mantle melting will require further data for other important crystalline phases to derive bulk incompatibilities as a function of residual mantle composition. In terms of radiogenic parents, Ar appears only slightly more incompatible than K in cpx (Fig. 3d), and it remains to be seen how He (possibly not controlled by the M2 site) behaves relative to U and Th. However, partitioning measurements for natural samples and our preliminary experimental results[18] suggest a D_{Ar} for olivine that is similar to, or higher than, the D_{Ar} in cpx, whilst K, U and Th would be expected to be relatively more incompatible[23]. If D_{He} in olivine were also to plot on an open parabola within an order of magnitude of D_{Ar}, these results would not support the long-standing assumption that noble gases are *de facto* more incompatible than their radioactive parents during mantle melting. Although the curvature of the noble-gas parabola for the M2 site in cpx indicates little fractionation between the noble gases regardless of size, the possibility of interstitial locations for He, or partitioning control by an alternative site (for example, M1 in cpx), could explain the observed fractionation of He (and Ne) from heavier noble gases in some MORB lavas[14]. □

Methods

Experiments

Details of piston-cylinder (1.0–3.0 GPa) and multi-anvil experiments (5.6–8.1 GPa) can be found in ref. 19, along with descriptions of the UVLAMP analytical technique. Additional 0.1-GPa experiments were performed in a rapid-quench TZM cold-seal apparatus, with a mixture of He, Ne, Ar, Kr and Xe as the pressure medium. Starting materials for TZM experiments were glasses of Albite:Diopside composition (50:50 for RB582 and 60:40 for RB586), taken above the liquidus to 1,300 °C for 6 h, then cooled to 1,250 and 1,200 °C, respectively, at 0.6 °C h^{-1}. The resultant cpx crystals are elongated and usually skeletal with numerous melt tubes along the central axis, but have large enough melt-free areas to allow square ablation pits of 50–100 μm a side. Accidental inclusion of melt in the analysis produces high partition coefficients, and the values used in this study are the average of the lowest 2–3 derived partition coefficients[19]. Note that current UVLAMP measurements for He are not considered accurate enough to be included in this study.

Simulations

The atomistic calculations allow explicitly for ionic relaxation surrounding the incorporated atom(s). Defect energies were calculated using GULP[24] and the conventional two-region approach with an inner region comprising typically 500 ions. A consistent set of interionic potentials[21] was used. For argon–oxygen interactions, Lennard–Jones potentials were derived by fitting to experimental absorption isotherms[25,26] in three zeolites—silicalite, mordenite and 5 A—using grand-canonical Monte Carlo[27]. Potentials for other noble gases were obtained using the usual scaling rules. As a test, the resulting potentials for Xe produced an absorption isotherm for silicalite in excellent agreement with experiment[28]. Lennard–Jones ε parameters for Ne–O, Ar–O, Kr–O and Xe–O were 60.073, 110, 125.1207 and 147.0658 K respectively; σ values were 2.7491, 3.0566, 3.2991 and 3.4841 Å. All calculations are in the static limit, and as a result are representative of extremely low temperatures. We use the defect energies to calculate solution energies[21], and we do not determine partition coefficients between solid and melt directly. These classical simulations cannot be extended to He owing to quantum effects.

Solution energies for substitution reactions in jadeite were calculated assuming, as previously[21], that the environment of the displaced Na^+ or Al^{3+} ions in the melt is the same as that in the relevant binary oxide. In Fig. 2, the 1 − effective site charge for the noble-gas atom on the Na(M2) site was compensated by exchanging Ti^{4+} for Al^{3+} on the M1 site. In Fig. 3, the lowest-energy, plausible charge-compensation mechanism for each valence was chosen as follows. For jadeite; noble gases = Ti(M1), 1 + not required, 2 + = Mg(M2), 3 + = Li(M1), 4 + = Li(M1) + Mg(M1). For diopside; noble gases = Sc(MgM1), 1 + = Lu(MgM1), 2 + not required, 3 + = Na(CaM1), 4 + = 2Na(CaM1).

Lattice strain model

According to the Blundy and Wood[9] adaptation of the Brice equation[22], the partition coefficient, D_i, for an ion with charge $n+$ and radius r_i entering crystal lattice site M can be described in terms of three parameters ($r^{n+}_{0(M)}$, the ideal radius of that site for cations with this charge; E^{n+}_M, the apparent (effective) Young's modulus of the site; and $D^{n+}_{0(M)}$, the 'strain-free' partition coefficient for a (fictive) ion with radius $r^{n+}_{0(M)}$) according to the expression:

$$D_i = D^{n+}_{0(M)} \times \exp\left\{\frac{-4\pi N_A E^{n+}_M \left[\frac{1}{2} r^{n+}_{0(M)}(r_i - r^{n+}_{0(M)})^2 + \frac{1}{3}(r_i - r^{n+}_{0(M)})^3\right]}{RT}\right\}$$

where N_A is the Avogadro constant, R the gas constant and T is in K. $D^{n+}_{0(M)}$ and E^{n+}_M vary with charge $n+$ and are pressure, temperature and melt-composition dependent, currently requiring experimental calibration[9].

Received 15 January; accepted 22 April 2003; doi:10.1038/nature01708.

1. Allègre, C. J., Staudacher, T. & Sarda, P. Rare gas systematics: Formation of the atmosphere, evolution and structure of the Earth's mantle. *Earth Planet. Sci. Lett.* **81,** 127–150 (1987).
2. Allègre, C. J., Hofmann, A. & O'Nions, K. The argon constraints on mantle structure. *Geophys. Res. Lett.* **23,** 3555–3557 (1996).
3. Harper, L. C. & Jacobsen, S. B. Noble gases and Earth's accretion. *Science* **273,** 1814–1818 (1996).
4. Turner, G. The outgassing history of the Earth's atmosphere. *J. Geol. Soc. Lond.* **146,** 147–154 (1989).
5. Broadhurst, C. L., Drake, M. J., Hagee, B. E. & Bernatowicz, T. J. Solubility and partitioning of Ar in anorthite, diopside, forsterite, spinel, and synthetic basaltic liquids. *Geochim. Cosmochim. Acta* **54,** 299–309 (1990).
6. Hiyagon, H. & Ozima, M. Partition of noble gases between olivine and basalt melt. *Geochim. Cosmochim. Acta* **50,** 2045–2057 (1986).
7. Broadhurst, C. L., Drake, M. J., Hagee, B. E. & Bernatowicz, T. J. Solubility and partitioning of Ne, Ar, Kr, and Xe in minerals and synthetic basalt melts. *Geochim. Cosmochim. Acta* **56,** 709–723 (1992).
8. Shibata, T., Takahashi, E. & Ozima, M. in *Noble Gas Geochemistry and Cosmochemistry* (ed. Matsuda, J.-I.)) 343–354 (Terra Science, Tokyo, 1994).
9. Blundy, J. D. & Wood, B. J. Prediction of crystal-melt partition coefficients from elastic moduli. *Nature* **372,** 452–454 (1994).
10. Wood, B. J. & Blundy, J. D. The effect of cation charge on crystal-melt partitioning of trace elements. *Earth Planet. Sci. Lett.* **188,** 59–71 (2001).
11. Van Keken, P. F. & Ballentine, C. J. Dynamical models of mantle volatile evolution and the role of phase transitions and temperature-dependent rheology. *J. Geophys. Res.* **104,** 7137–7151 (1999).
12. Van der Hilst, R. D., Widiyantoro, S. & Engdahl, E. R. Evidence for deep mantle circulation from global tomography. *Nature* **386,** 578–584 (1997).
13. O'Nions, R. K. & Oxburgh, E. R. Heat and helium in the Earth. *Nature* **306,** 429–431 (1983).
14. Ozima, M. & Igarashi, G. T. The primordial noble gases in the Earth: A key constraint on Earth evolution models. *Earth Planet. Sci. Lett.* **176,** 219–232 (2000).
15. Anderson, D. L. A statistical test of the two reservoir model for helium. *Earth Planet. Sci. Lett.* **193,** 77–82 (2001).
16. Marty, B. & Lussiez, P. Constraints on rare gas partition coefficients from analysis of olivine-glass from a picritic mid-ocean ridge basalt. *Chem. Geol.* **106,** 1–7 (1993).
17. Valbracht, P. J., Honda, M., Staudigel, H., McDougall, I. & Trost, A. P. in *Noble Gas Geochemistry and Cosmochemistry* (ed. Matsuda, J.-I.)) 373–381 (Terra Science, Tokyo, 1994).
18. Brooker, R. A., Wartho, J.-A., Carroll, M. R., Kelley, S. P. & Draper, D. S. Preliminary UVLAMP determinations of argon partition coefficients for olivine and clinopyroxene grown from silicate melts. *Chem. Geol.* **147,** 185–200 (1998).
19. Chamorro, E. M. *et al.* Ar and K partitioning between clinopyroxene and silicate melt to 8 GPa. *Geochim. Cosmochim. Acta* **66,** 507–519 (2002).
20. Hiyagon, H. Constraints on rare gas partition coefficients from analysis of olivine-glass from a picritic mid-ocean ridge basalt—Comments. *Chem. Geol.* **112,** 119–122 (1994).
21. Allan, N. L., Blundy, J. D., Purton, J. A., Lavrentiev, M. Y. & Wood, B. J. in *EMU Notes in Mineralogy* (ed. Geiger, C. A.)) **Vol. 3** 251–302 (Eötvös Univ. Press, Budapest, 2001).
22. Brice, J. C. Some thermodynamic aspects of the growth of strained crystals. *J. Crystal Growth* **28,** 249–253 (1975).
23. Beattie, P. The generation of uranium series disequilibrium by partial melting of spinel peridotite: Constraints from partitioning studies. *Earth Planet. Sci. Lett.* **117,** 379–391 (1993).
24. Gale, J. D. GULP: A computer program for the symmetry-adapted simulation of solids. *J. Chem. Soc. Faraday Trans.* **93,** 629–637 (1997).
25. Watanabe, K., Austin, N. & Stapleton, M. R. Investigation of the air separation properties of zeolite types A, X and Y by Monte Carlo simulation. *Mol. Simulat.* **15,** 197–221 (1995).
26. Macedonia, M. D., Moore, D. D. & Maginn, E. J. Adsorption studies of methane, ethane, and argon in zeolite mordenite: Molecular simulations and experiments. *Langmuir* **16,** 3823–3834 (2000).
27. Frenkel, D. & Smit, B. *Understanding Molecular Simulation* (Academic, San Diego, 1996).
28. Pellenq, R. J. M. & Nicholson, D. Grand ensemble Monte Carlo simulation of simple molecules adsorbed in silicalite-zeolite. *Langmuir* **11,** 1626–1635 (1995).
29. Zhang, Y. & Xu, Z. Atomic radii of noble gas elements in condensed phases. *Am. Mineral.* **80,** 670–675 (1995).
30. Onuma, N., Higuchi, H., Wakita, H. & Nagasawa, H. Trace element partition between two pyroxenes and the host lava. *Earth Planet. Sci. Lett.* **5,** 47–51 (1968).
31. Shannon, R. D. Revised effective radii and systematic studies of interatomic distances in halides and chalcogenides. *Acta Crystallogr. A* **32,** 751–767 (1976).

Supplementary Information accompanies the paper on **www.nature.com/nature**.

Acknowledgements We thank J. Craven and R. Hinton for analytical assistance with the Edinburgh ion-probe; we also thank M. Carroll for originally inspiring the idea of a 'flat' parabola, and J. Jones for comments. This work was supported by the NERC, and by research fellowships from the Royal Society, the European Commission and the Leverhulme Trust.

Competing interests statement The authors declare that they have no competing financial interests.

Correspondence and requests for materials should be addressed to R.A.B. (r.a.brooker@bristol.ac.uk).